Seasonal differences in future climate and streamflow variation in a watershed of Northern China

Article *in* Journal of Hydrology: Regional Studies · October 2021

DOI: 10.1016/j.ejrh.2021.100959

Wenxu Cao
Beijing Forestry University

Zhi-Qiang Zhang
Beijing Forestry University

Larry Band
University of North Carolina at Chapel Hill

Shengping Wang
North China Electric Power University

Journal of Hydrology: Regional Studies 38 (2021) 100959

Contents lists available at ScienceDirect

Journal of Hydrology: Regional Studies

journal homepage: www.elsevier.com/locate/ejrh

Seasonal differences in future climate and streamflow variation in a watershed of Northern China

Wenxu Cao[a,b,c], Zhiqiang Zhang[a,b,c,*], Yongqiang Liu[d], Lawrence E. Band[e], Shengping Wang[f], Hang Xu[a,b,c]

[a] College of Soil and Water Conservation, Beijing Forestry University, Beijing 100083, PR China
[b] Key Lab. Soil & Water Conservation, The State Forestry and Grassland Administration, Beijing 100083, PR China
[c] Beijing Engineering Research Center for Soil & Water Conservation, Beijing Commission of Science and Technology, Beijing 100083, PR China
[d] Center for Forest Disturbance Science, Southern Research Station, USDA Forest Service, Athens, GA 30602, USA
[e] Department of Environmental Sciences, University of Virginia, Charlottesville, VA 22904, USA
[f] College of Hydraulic and Hydro-Power Engineering, North China Electric Power University, Beijing 102206, PR China

A R T I C L E I N F O

Keywords:
Climate change
Hydrological regime
RHESSys
Summer season
Return period
Watershed management

A B S T R A C T

Study region: The Chaohe watershed is a meso-scale watershed in northern China, and the primary reservoir watershed for Beijing's drinking water supply.
Study focus: This research aims to evaluate the effects of climate change on future seasonal streamflow regimes and understand the challenges to watershed management. The Regional Hydro-Ecological Simulation System (RHESSys) was applied to investigate the watershed's future hydrographic characteristics under the forcing of the downscaled precipitation and temperature projected by General Circulation Models (GCMs) under three emissions scenarios.
New hydrological insights for the region: The future climate exhibits a drier and warmer trend in the summer monsoon period contrasting with other seasons in the watershed. Precipitation will decrease by 47.5–57.2 mm during the summer monsoon period while increasing annually. Future summer streamflow will decrease accordingly, which is also driven by increased evapotranspiration due to rising temperature. An increased dispersion coefficient of streamflow also indicates more dramatic variations in summer. The annual streamflow magnitude with a 5-year return period increases significantly ($p < 0.01$), indicating a reduced risk for future water shortages. However, the magnitude of streamflow will decrease with the prolonged return periods ($p < 0.01$). This study emphasizes the critical significance of predicting the seasonal variability of streamflow and other hydrological property changes at the local scale to provide valuable information for developing adaptive resource management and hazard relief strategies.

1. Introduction

Climate change accelerates the global water cycle, alters flow regime, induces more extreme events (López-Ballesteros et al., 2020), and modifies regional and global water resource distributions (Piao et al., 2010; Gizaw et al., 2017). However, there are significant discrepancies in climate change between different geographical regions and time scales (Blöschl et al., 2019). More complex

* Correspondence to: College of Soil and Water Conservation, Beijing Forestry University, Qinghua East Road 35#, Haidian District, Beijing 100083, PR China.
E-mail address: Zhqzhang@bjfu.edu.cn (Z. Zhang).

https://doi.org/10.1016/j.ejrh.2021.100959
Received 6 July 2021; Received in revised form 28 October 2021; Accepted 30 October 2021
2214-5818/

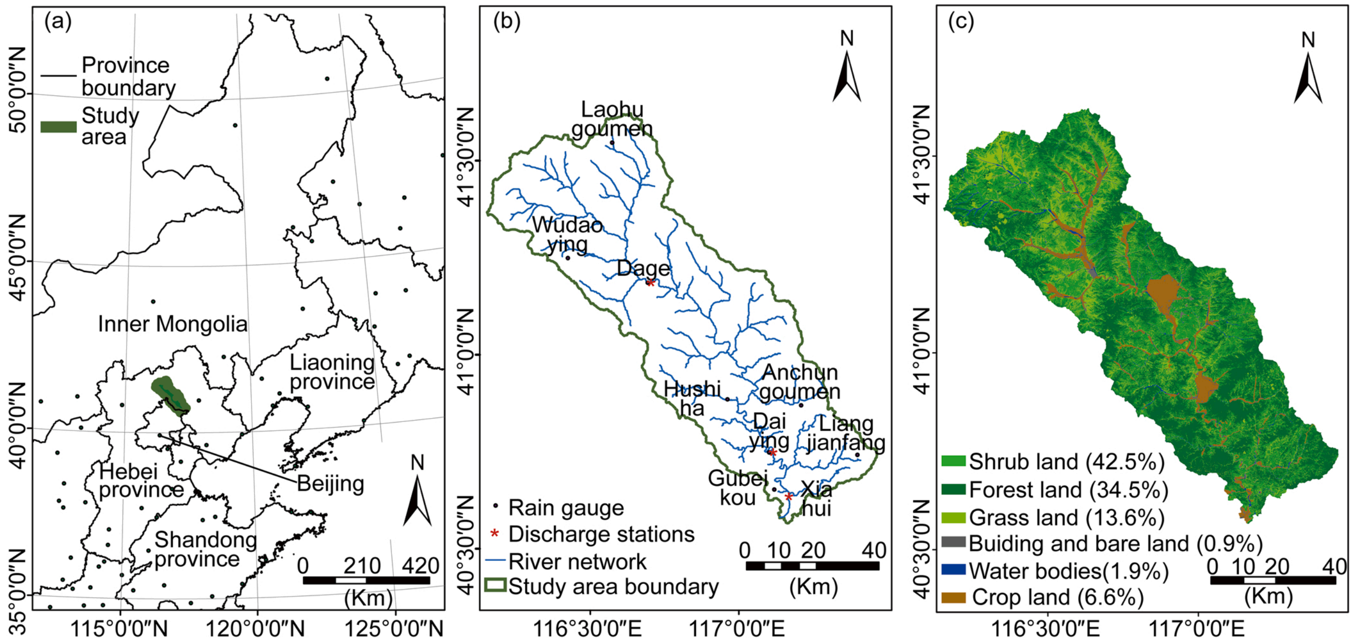

Fig. 1. Geographic information of the study area: (a) location of the Chaohe watershed and adjacent provinces in China, (b) location of the hydro-meteorological stations, and (c) land use within the watershed in 2009.

heterogeneous precipitation changes than the consistent warming trend will cause divergent fluctuations within hydrological processes across the scales (Donat et al., 2016). For instance, precipitation substantially increased in the southwestern China, but declined by 5% per decade in the northern region (Zhai et al., 2005). Extreme flows, such as high flows and low flows, are expected to rise within northern Europe and the high latitude regions of North America, whereas a decrease in the southern regions of Europe and North America (Dai et al., 2009; Hirabayashi et al., 2013). Streamflow is projected to decrease over the southwestern North America in the next 100 years, while the opposite trend is predicted over the eastern North America due to the increased precipitation (Reynolds et al., 2015). The discrepancies in climate change and its hydrological impacts make it hard to develop adaptive watershed management without localized projections.

The East Asian summer monsoon (EASM) transfers moisture to land from the ocean facilitating temporal heterogeneity in precipitation. The EASM has been weakening for the last half-century, leading to drier conditions over northern China's semi-arid areas (Shen et al., 2018). Since the late 1990s, a significant trend towards drier parts of northern China has been noticed, which played an essential role in modifying the drought pattern (Xu et al., 2018). More importantly, the monsoon system generates seasonal changes in climate and thus hydrological regimes. For instance, significant decreasing trends in the summer precipitation were detected over northern China, while the opposite trend was found for the same area in the winter months (Zhai et al., 2005). Temporal variability in climate and streamflow have significant consequences for regional water resources management (Seddon et al., 2016). Climatic change-induced seasonal fluctuations in climate and hydrological regimes pose severe challenges to disaster avoidance in northern China. It is estimated that extreme drought in Northwest China has caused major ecological and economic consequences (Ouyang et al., 2015). Therefore, it is important to detect the variations in the hydrological regime driven by climate change at different temporal scales (i.e., both annual and seasonal) at the watershed scale to achieve sustainable water resources management and adaptation strategies in the future.

The effects of climate change on water resources can be investigated by incorporating climate change projections (e.g., air temperature and precipitation) into models that reliably quantify the spatio-temporal variations of water fluxes in a watershed under different socioeconomic pathways (Aloysius and Saiers, 2017). General Circulation Models (GCMs) are applied to provide estimates of the climate response and future climate scenarios over large regions (Asseng et al., 2013). The number of GCMs available for climate change projections is increased from 25 with the Coupled Model Inter-comparison Project (CMIP) Phase 3 to 61 with CMIP Phase 5. However, uncertainties in predicting the future climate remain large and might even increase with the increasing number of climate models available (Hargreaves, 2010; Lutz et al., 2016). Additionally, the performance of GCMs varies within geographic regions (Ahmadalipour et al., 2017). Therefore, it is vital to select the appropriate GCMs to capture and forecast the climatological patterns and variations for a specific region. At regional and watershed scales, GCMs must be downscaled to generate the accurate high-resolution climate variables used for hydrological simulation and prediction. Although GCMs could generate hydrological variables directly, the simulated hydrological processes and regimes are inadequate (Xu and Singh, 2004). For example, GCMs do not represent the lateral transfer of water fluxes very well (Kite et al., 1994). Physical processes-based, distributed hydrological models could dynamically simulate the transfer of horizontal and vertical water fluxes by dividing watershed into grids or sub-catchments and incorporating watershed physical characteristics (Fatichi et al., 2016; Tegegne et al., 2017). Hence, such models have been used in hydrological simulations under various scenarios, including changes in land use and land cover, and climate change (Zheng et al., 2018).

This study aims to predict the future hydrological regimes in the Chaohe watershed, situated in the temperate East Asian monsoon climate region of northern China. We used downscaled GCMs data to forecast future climate change and drive the process-based distributed eco-hydrological model RHESSys. Our specific objectives are to (1) project the annual and monthly variations in precipitation and air temperature, (2) simulate the responses of annual and seasonal streamflow dynamics under future climate scenarios, and (3) evaluate the hydrological regime changes and forecast the risks for hydrological management at the study watershed.

2. Study region, data, and methods

2.1. The Chaohe watershed

The Chaohe watershed located in northern China (116°08'–117°28′E, 40°34′–41°37′N, Fig. 1a) has a drainage area of 4854.8 km^2 elevated between 159 and 2218 m above the sea level. This watershed, the essential water source region of Miyun Reservoir, provides more than 70% of the drinking water for the urban population in Beijing (Tang et al., 2011). The watershed is dominated by brown loam and luvic cinnamon soils (Li et al., 2010). In addition, more than 80% of the watershed is covered by forests, shrubs, and grass (Fig. 1c), while the rest is used for crop and construction or as bared areas. The mean annual temperature (MAT) and precipitation (MAP) during 1961–2015 is 12.3 ℃ and 509.2 mm, respectively. As a unique feature of the monsoon climate, the summer is warm and wet, contributing more than 80% of the annual precipitation.

2.2. Data

Daily precipitation series (1961–2015) from eight precipitation monitoring sites (Fig. 1b) were attained by the Haihe River Water Conservancy Commission, Beijing Water Authority, and Hydrology and Water Resource Survey Bureau of Hebei Province. The Thiessen polygon method was used to calculate the annual average precipitation (Thiessen, 1911). In addition, daily minimum, mean, and maximum temperature during 1961–2015 (representing the historical period) were obtained from three national meteorological stations (Miyun, Fengning, and Chengde) maintained by the State Meteorological Administration, China. Daily streamflow data at Xiahui Hydrological Station (the outlet station of the watershed, Fig. 1b) were obtained from the same source for daily precipitation

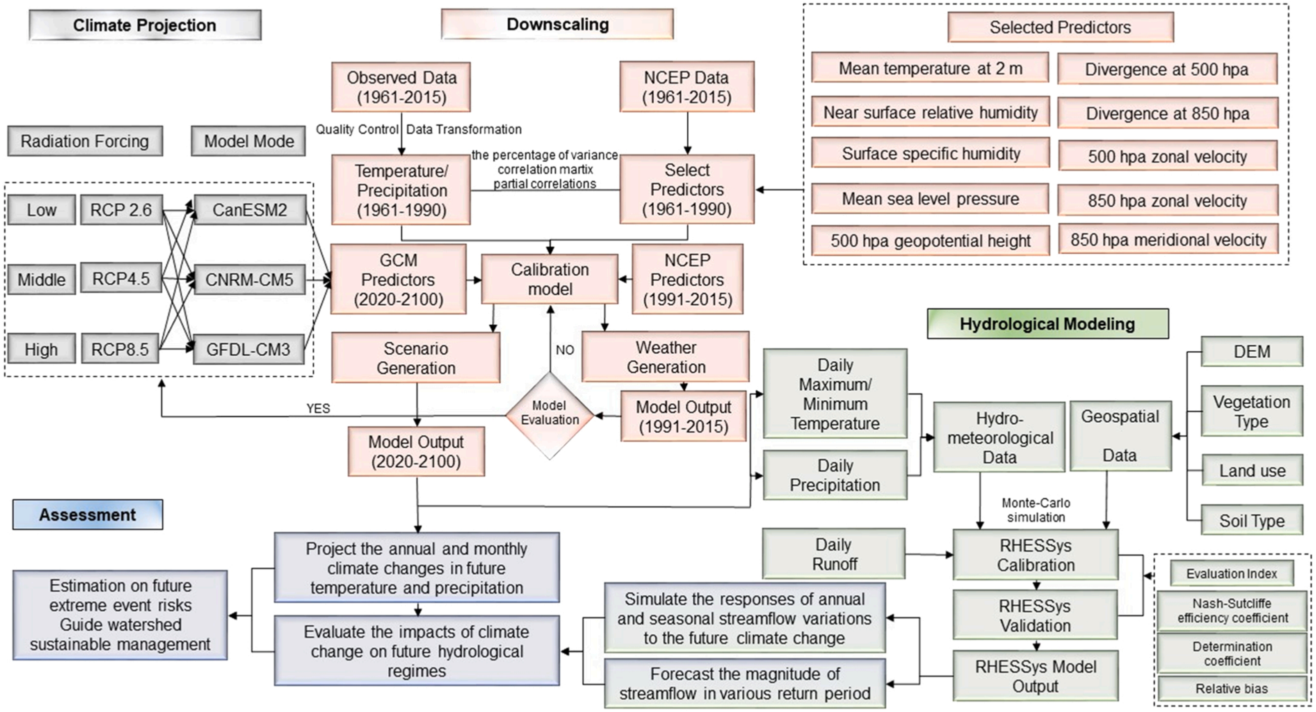

Fig. 2. The schematic diagram of the analytical procedures and techniques used in this study.

data (Cao et al., 2018; Lou et al., 2015).

The digital elevation model (DEM) and land use maps for 1979, 1989, 1999, and 2009 with 30 m resolution were derived from the Computer Network Information Center and Institute of Remote Sensing and Digital Earth (http://www.ceode.cas.cn/sjyhfw/), Chinese Academy of Sciences, respectively. The River network was built up by calculating flow direction from the DEM data using the eight flow directions (D8) algorithm (O'Callaghan and Mark, 1984). The DEM specified flow directions by assigning flow from each pixel to one of its eight neighbors in the direction with the steepest downward slope. Soil information was derived from the Environmental and Ecological Science Data Center for western China (Wang et al., 2013). Finally, land use data were reclassified into the evergreen forest, deciduous forest, shrub, grass, agriculture land, and undeveloped land according to RHESSys land cover database requirements.

2.3. Scenario datasets and downscaling

The present and future daily precipitation and temperature projected by GCMs were obtained from the Earth System Grid Federation (ESGF, http://esgf-node.llnl.gov/search/cmip5/). An increasing number of climate models are available predicting important climatic variables. For example, the Coupled Model Inter-comparison Project Phase 5 involves outputs from 61 different GCMs (Lutz et al., 2016). Many GCMs such as CanESM2, CNRM-CM5, and GFDL-CM3 can realistically capture China's climatological patterns and spatial variations (Yang, 2014). The CanESM2 model is widely used because readily available daily predictor variables can be directly fed into the Statistical Downscaling Model (SDSM). Thus, a decision support tool for assessing local climate change effects and the model outputs can be applied for further impact analysis with a high degree of certainty under new sets of emission scenarios downscaled by the SDSM (Getachew et al., 2021). Previous evaluation studies indicated that the CanESM2 and GFDL-CM3 could realistically reproduce the observed seasonal precipitation by national weather stations over northern China (Chen and Frauenfeld, 2014). In addition, the CNRM-CM5 also shows higher accuracy than the other models in simulating spatial patterns in the decadal change of climate zones over China (He et al., 2019). The selected CMIP5 GCMs (including GFDL-CM3, CanESM2, and CNRM-CM5, Fig. 2) were found to be able to reproduce climate variability (i.e., statistical methods of annual average, monthly average, correlation coefficient, and percent bias, Fig. S1 and S2) in the study area during calibration and validation. Moreover, three Representative Concentration Pathways (RCP) scenarios (i.e., RCP8.5, RCP4.5, and RCP2.6) representing distinct radiative forcing levels were applied to reflect the high, medium stabilization, and mitigation emission scenario, respectively (Moss et al., 2010). All data were uniformly interpolated to identical resolution with the US National Oceanic and Atmospheric Administration National Centers for Environmental Prediction reanalysis data.

The SDSM was used to generate the regional climate data for our study area. The SDSM was selected based on the model's excellent climate downscaling techniques (Liu et al., 2021). First, long-term and high-quality observation data (1961–2015) was used to establish the robust statistical relationship between large-scale downscaling predictor variables (i.e., GCMs predictors) and local climate variables (i.e., observed temperature and precipitation) over the study area. This step was needed to develop the statistical downscaling method. Second, the SDSM combined two primary statistical downscaling transfer function generators that relate large-area climate to local weather or from the upper air to the ground weather (Wilby and Wigley, 1997). The first method includes applying efficient regression analysis, and the second is used to produce a temporary series of local variables such as precipitation with high stochastic fluctuations. Thirdly, the SDSM is especially effective for hydrological research (Wilby, 2002). As indicated in many evaluation studies, this method replicated the main features of the observed hydrometeorology (Liu et al., 2021). The goal of the SDSM is to establish the empirical relationship between the local climate variables and large-scale variables. This study selected different predictors, including mean temperature, relative and specific humidity near the ground surface, and mean sea level pressure for temperature downscaling (Table 1 and S1). Meanwhile, we chose the 500 hPa geopotential height, divergence, and zonal velocity for precipitation downscaling (Table S1). We used the conventional bias correction method within the SDSM to inflate the variance of the downscaled time series. Finally, we split the historical period of 1961–2015 into a calibration period (i.e., 1961–1990) and the validation period (i.e., 1991–2015). The detailed downscaling process was implemented in the following steps:

(1) Quality control and transformation for observed temperature and precipitation data. Enable the diagnosis of missing data and outliers in observed precipitation and temperature data before running the SDSM.
(2) Selecting suitable downscaling predictors. The observed temperature and precipitation data were used to screen the preferred predictors for precipitation, minimum and maximum temperature in the Chaohe watershed, respectively. Finally, we selected ten predictors: mean temperature, relative and specific humidity near the ground surface, mean sea level pressure, and geopotential height. The details are described in Table S1.

Table 1
List of the daily predictor variables selected in the Chaohe watershed.

Description	Predictors	Description	Predictors
Mean temperature at 2 m	Temp	Divergence at 500 hPa	P5zh
Near-surface relative humidity	Rhum	Divergence at 850 hPa	P8zh
Surface specific humidity	Shum	500 hPa zonal velocity	P5_u
Mean sea level pressure	Mslp	850 hPa zonal velocity	P8_u
500 hPa geopotential height	P500	850 hPa meridional velocity	P8_v

(3) Calibrating and validating the SDSM. The daily temperature and precipitation data and selected predictors were used to construct downscaling multiple regression equations.
(4) Generating the daily weather series for the next eighty years based on the selected GCMs under the three emission scenarios. Although 2020 is no longer a future year, it is included in the future period for the convenience of analysis.

2.4. Regional Hydro-Ecological Simulation System model

2.4.1. Model construction and parameterization

The Regional Hydro-Ecological Simulation System (RHESSys), a process-based distributed model, was used in our study to project the future streamflow variation. The RHESSys represents watersheds in a spatially nested hierarchical structure with a range of meteorological and hydrological processes associated with different hierarchy levels (Fig. S3). The RHESSys model includes an explicit hillslope hydrology model linking the ecosystem patches in a catena, resolving coupled water, carbon, and nitrogen cycling with spatially varying topo-climate drivers (Tague et al., 2008). Specifically, the soil water profile is depicted in a vertically three-layer model, covering a saturated zone, an unsaturated zone, and a surface detention zone (Tague and Band, 2004). The standard Penman-Monteith approach is used to calculate evaporation and transpiration rates. Stomatal conductance is used for surface conductance in a multiplicative model (Jarvis, 1976). Stomatal conductance is driven by solar radiation, vapor pressure deficit, rooting zone soil moisture, air CO_2 concentration, and air temperature controls. The RHESSys further scales leaf-level transpiration to canopy transpiration by integrating over the leaf area index (LAI). Canopy interception is a function of the water-holding capacity of the vegetation. Net throughfall from the canopy is first added to surface detention storage and then allowed to infiltrate into the soil following Phillip's infiltration (Philip, 1957). A condensed description of the hydrological processes, including interception, transpiration, and evaporation is shown in the following equation. A more detailed description of the RHESSys can be found in the literature (Band et al., 1996; Tague et al., 2004).

Infiltration in RHESSys is calculated by Phillip equation:

$$q_{infil} = It_p + S_p\sqrt{t_d + t_p} + K_{sat}\left(t_d - t_p\right) \quad \text{for} \quad t_d > t_p \tag{1}$$

$$q_{infil} = It_d \quad \text{for} \quad t_d < t_p \tag{2}$$

$$S_p = \sqrt{2}K_{sat}0.76\varphi_{ae} \tag{3}$$

$$K_{sat}(\mathrm{z}) = K_{sat\_0}exp^{\left(-\frac{z}{m}\right)} \tag{4}$$

$$t_p = K_{sat}0.76\varphi_{ae}\frac{(\Phi - \theta_0)}{I(I - K_{sat})} \tag{5}$$

where q_{infil} is infiltration; I and t_d are input intensity and duration; t_p is the time to ponding; K_{sat} is saturated hydraulic conductivity defined by the saturation depth z; K_{sat_0} is hydraulic conductivity at the surface, and m describes the decay rate of conductivity with depth; S_p is sorptivity; φ_{ae} is air entry pressure; Φ is porosity, and θ_0 is initial soil moisture content.

Evaporation and transpiration rates are computed using the standard Penman-Monteith equation. Evapotranspiration rates are computed for rainy and dry periods of each day, and the vapor pressure deficit is adjusted accordingly. Total daily evaporation (E) is computed as:

$$E = \min\left[\theta_I, E(vpd = 0; g_s)(D_{rain}) + E\left(vpd = \overline{vpd}; g_s\right)\left(D_{day} - D_{rain}\right)\right] \tag{6}$$

where θ_I is the interception storage; vpd is the daily vapor pressure deficit; D_{rain} is the rain duration; D_{day} is the day length; g_s is the nonvascular stratum conductance.

Total transpiration T_c is computed as:

$$T_c = E(vpd = 0; gs_{sun}) + E(vpd = 0; gs_{shade})(D_{rain})$$
$$+ E\left(vpd = \overline{vpd}; gs_{sun}\right) + E\left(vpd = \overline{vpd}; gs_{shade}\right)\left(D_{day} - D_{rain}\right) \tag{7}$$

where gs_{sun} and gs_{shade} are the canopy conductance for sun and shaded leaves.

2.4.2. Model calibration and validation

The RHESSys was run with a daily time step based on available meteorological data. Our previous studies indicated an abrupt change in streamflow in the late 1980 s occurred due to implementing large-scale afforestation programs (Zheng et al., 2015; Wang et al., 2013). Therefore, we chose streamflow data from 1961 to 1979 and land use data of 1979 to calibrate the RHESSys model to avoid influence from human activities. First, two years (i.e., 1961–1962) of data were selected to spin up this model. The model was validated using the calibrated parameters, land use data in 2009, and hydro-meteorological data from 2000 to 2015. The RHESSys relies on parameters to describe typical soil, vegetation, and land use characteristics. Literature-based estimates and the RHESSys parameter database (https://github.com/RHESSys/RHESSys/wiki/Parameter-Definition-Files) have been used to modify values for the vegetation and soil types in our study area. Seven key hydrologic parameters reflecting drainage efficiency and storage capacity of soils required calibration and validation, including vertical and horizontal saturated hydraulic conductivity (K_{sat_v} and K_{sat_h}), decay of saturated hydraulic conductivity with depth (m), percentage of infiltrated water bypass to the deeper groundwater store (gw1), drainage rate of the groundwater (gw2), and soil depth (Tague et al., 2004). A Monte-Carlo simulation was implemented to sample 3000 initial parameter sets from recommended ranges in the RHESSys parameter database, and finally, the optimum parameter set was calibrated and validated (Table 2). In addition, the relative bias (B_{ias}), coefficient of determination (R^2), and Nash-Sutcliffe efficiency (N_{SE}, Nash and Sutcliffe, 1970) were applied to evaluate the model performances (Legates and Mccabe, 1999; Tong et al., 2014):

$$B_{ias} = \frac{\sum_{t=1}^{n}(O_t - S_t\quad)}{\sum_{t=1}^{n} S_t} \times 100\% \tag{8}$$

$$R^2 = \frac{\left[\sum_{t=1}^{n}\left(S_t - \overline{S}\right)\left(O_t - \overline{O}\right)\right]^2}{\sum_{t=1}^{n}\left(S_t - \overline{S}\right)^2\sum_{t=1}^{n}\left(O_t - \overline{O}\right)^2} \tag{9}$$

$$N_{SE} = 1 - \frac{\sum_{t=1}^{n}(S_t - O_t)^2}{\sum_{t=1}^{n}\left(O_t - \overline{O}\right)^2} \tag{10}$$

where S_t is the simulated data; O_t is the observed data; $\overline{S}$ and $\overline{O}$ are the average of the simulated and observed, respectively; n is the length of the time series in days.

The closer to 1 N_{SE} and R^2 are, the better the RHESSys model performs. Model performance is reliable when N_{SE} and R^2 are larger than 0.5 and 0.6, and B_{ias} is within ± 25%, respectively (Moriasi et al., 2013).

2.5. Analysis of streamflow changes

The dispersion coefficient (D_c) of streamflow was used to depict the stability of streamflow and calculated as follows (Zhang et al., 2016):

$$D_c = \frac{75^{th} - 25^{th}}{50^{th}} \times 100\% \tag{11}$$

where 25th, 50th, 75th are the annual streamflow percentiles. The flow duration curve was estimated to depict the frequency distribution of streamflow from high flow to drought events for 2020–2100 under the three RCPs. Return periods under five levels, including 100-year, 50-year, 20-year, 10-year, and 5-year, were applied to analyze streamflow frequency's temporal variation during the historical and future periods.

3. Results

3.1. Calibration and validation of GCM downscaling and RHESSys

To run the SDSM, we need to calibrate and validate the relationship between observed temperature/precipitation and large-scale predictors before future climate scenarios with the GCM outputs could be effectively downscaled. The scatter plots between downscaled and observed daily maximum, minimum temperature, and precipitation for the calibration and validation period are depicted in Fig. 3. The downscaled temperature data has been assessed to be generally consistent with observed historical data, although it somewhat overestimated the observed maximum (Figs. 3a and 3d) and minimum (Figs. 3b and 3e) temperatures in the upper end. In

Table 2
Calibrated model parameters scalar values for the RHESSys model.

Parameter	Definition	Initial Range	Optimal Value	Reference
Ksat_v	Vertical saturated hydraulic conductivity	1.00–150.00	112.27	(Tague et al., 2004)
Ksat_h	Horizontal saturated hydraulic conductivity	1.00–150.00	141.37	(Tague et al., 2004)
m_v	The decay of vertical K with depth	0.01–20.00	10.28	(Band et al., 2000)
m_h	The decay of lateral K with depth	0.01–20.00	1.05	(Band et al., 2000)
gw1	Percentage of infiltrated water bypass to the deeper groundwater store	0.001–0.30	0.21	(Tague et al., 2008)
gw2	Drainage rate of the groundwater	0.01–0.90	0.82	(Tague et al., 2008)
soil_depth	Soil depth	0.10–10.00	2.24	(Tague et al., 2008)

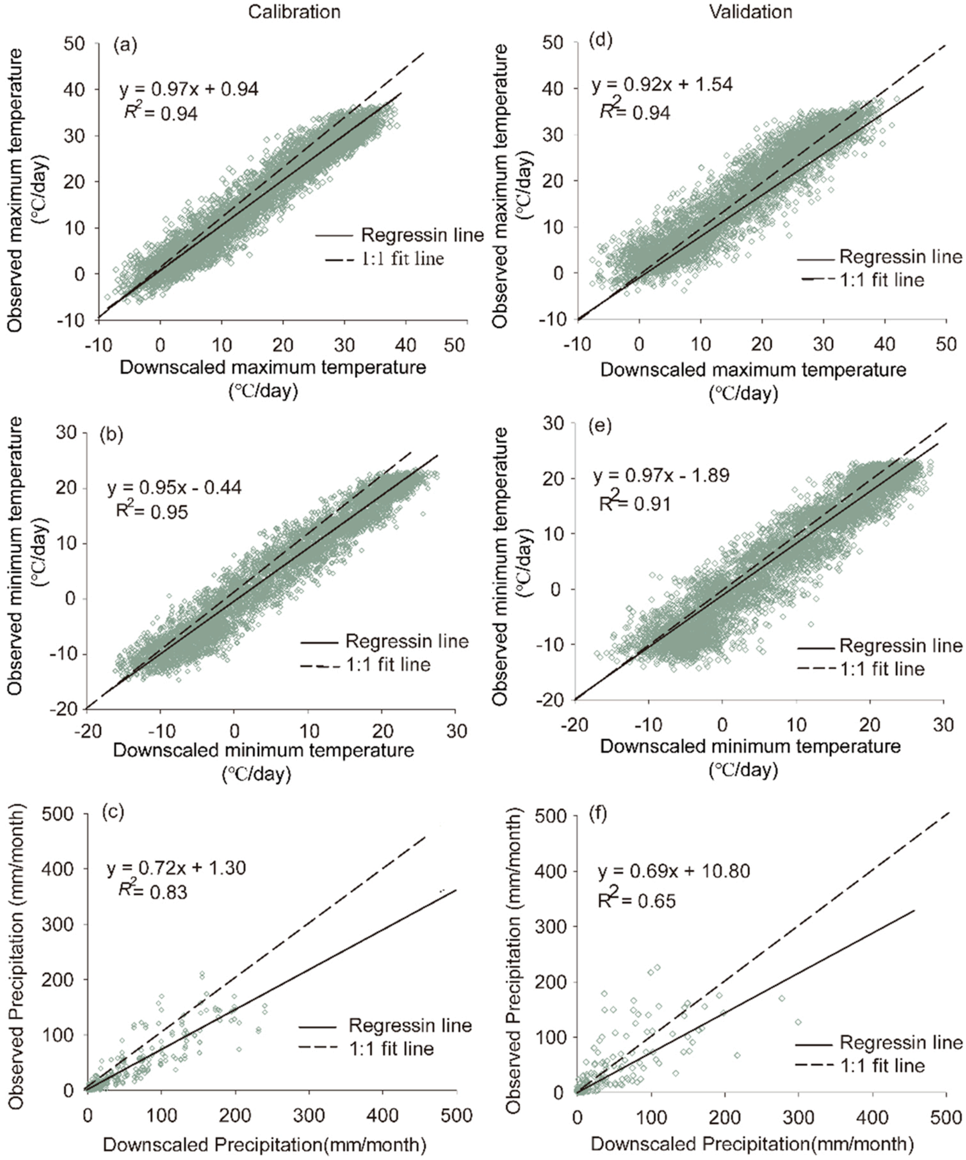

Fig. 3. Comparison of observed and GCM-downscaled maximum (a, d), minimum temperature (b, e), and precipitation (c, f) during the calibration (1961–1990) and validation (1991–2015) periods, respectively.

addition, downscaled precipitation was close to the observed values except for extreme conditions. Monthly precipitation was under-predicted for the values close to zero but over-predicted for large values during the calibration (Fig. 3c) and validation (Fig. 3f) periods. The downscaled maximum temperature, minimum temperature, and precipitation produced R^2 of 0.94, 0.95, and 0.83 during the calibration period. The values exhibited a little better than those in the verification period (i.e., 0.94, 0.91, and 0.65, respectively). Overall, the SDSM model was very capable of generating projected climate scenarios over the Chaohe watershed.

The values of R^2, N_{SE}, and B_{ias} during the RHESSys model calibration period were 0.87%, 0.86%, and 13.31%, respectively, indicating that the model performed exceptionally well to capture the hydrograph for the watershed (Fig. 4a). Calibrated soil parameters governing the hydrological processes include horizontal and vertical saturated hydraulic conductivity (i.e., Ksat_h and Ksat_v, respectively), decay of horizontal and vertical K with depth (i.e., m_h and m_v, respectively), groundwater bypass flow (i.e., gw1), and groundwater drainage rate (i.e., gw2). In addition, soil depth, a critical parameter for the hydrological process in the rocky mountain area of northern China, was also calibrated (Table 2).

Model validation further confirmed the modeling system's capacity to simulate the watershed's hydrological processes, although the values of R^2, N_{SE}, and B_{ias} declined slightly in the validation period to 0.76%, 0.74%, and 18.46%, respectively (Fig. 4b). As a result, there was a slight overestimate in the monthly streamflow with the RHESSys for the watershed. However, overall, the modeling system was able to reproduce the observed streamflow satisfactorily.

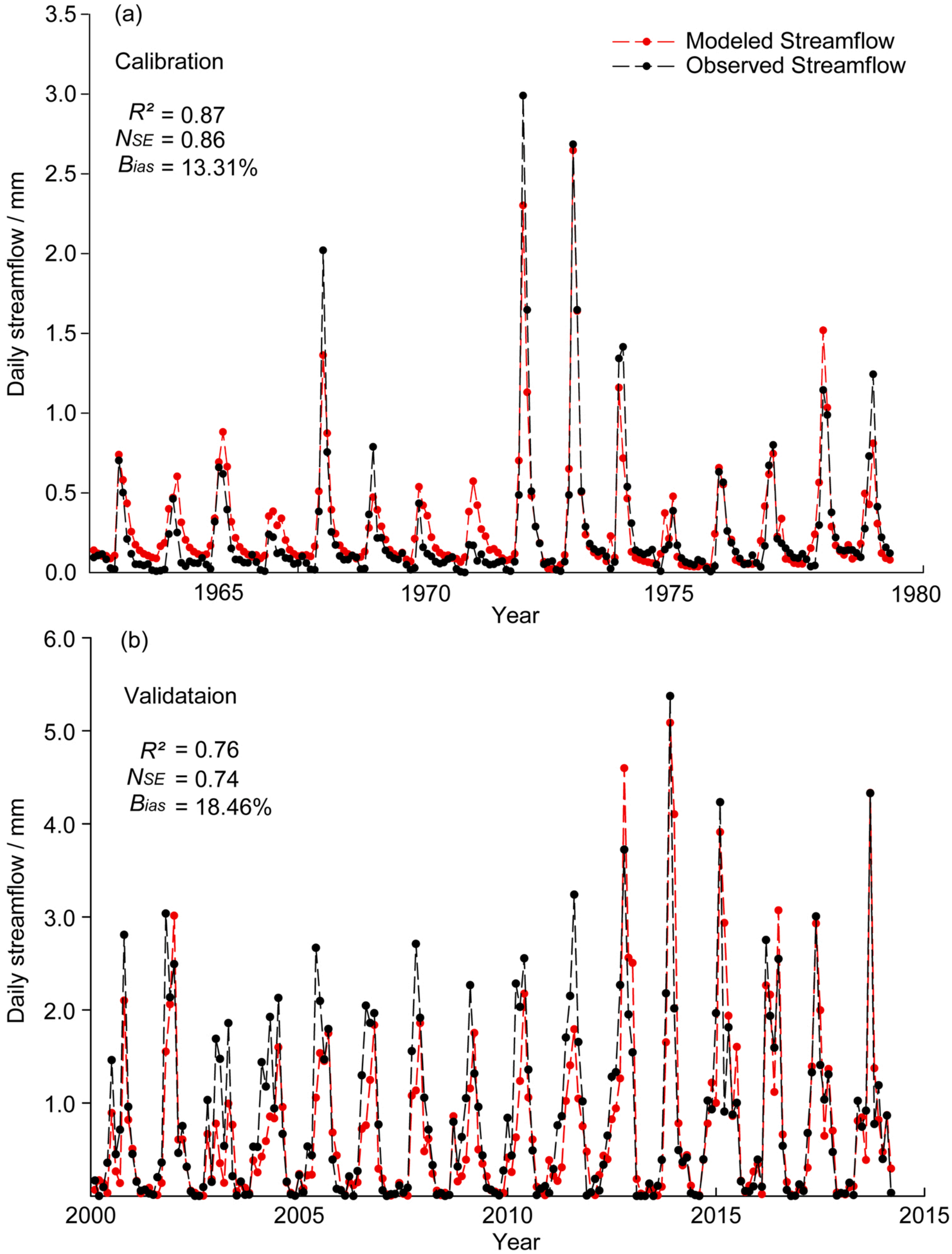

Fig. 4. RHESSys calibration (a) and validation (b) for monthly streamflow in the Chaohe watershed.

3.2. Future climate changes under three RCPs

3.2.1. Projected future temperature and precipitation changes

The projected annual temperature compared with the historical measurement is presented in Fig. 5a under all RCP scenarios across the study area. The MAT will increase significantly by 0.8 °C until 2100 under the RCP2.6 scenario, which is within one of the long-term temperature increase targets (i.e., below 1.5 °C from the 'pre-industrial' era until 2100). The temperature under the medium stabilization scenario is expected to increase by 1.6 °C, crossing the 1.5 °C threshold. MAT will rise by 3.8 °C under the high baseline emission pathway, which is beyond the threshold for keeping global warming below 2.0 °C. With the radiative forcing increasing, MAT under the RCP8.5 scenario shows the most significant warming (change by 31.2% compared with the historical period) than that increase under the medium (13.3%) and low-level (6.8%) emission scenarios. Moreover, an increasing trend of annual precipitation is projected for all three scenarios over the Chaohe watershed (Fig. 5b–d): relative to the mean annual precipitation (MAP) for the historical period 1961–2015, future MAP will increase by 10.3%, 9.6%, and 8.0% under the high, medium, and low- level emission

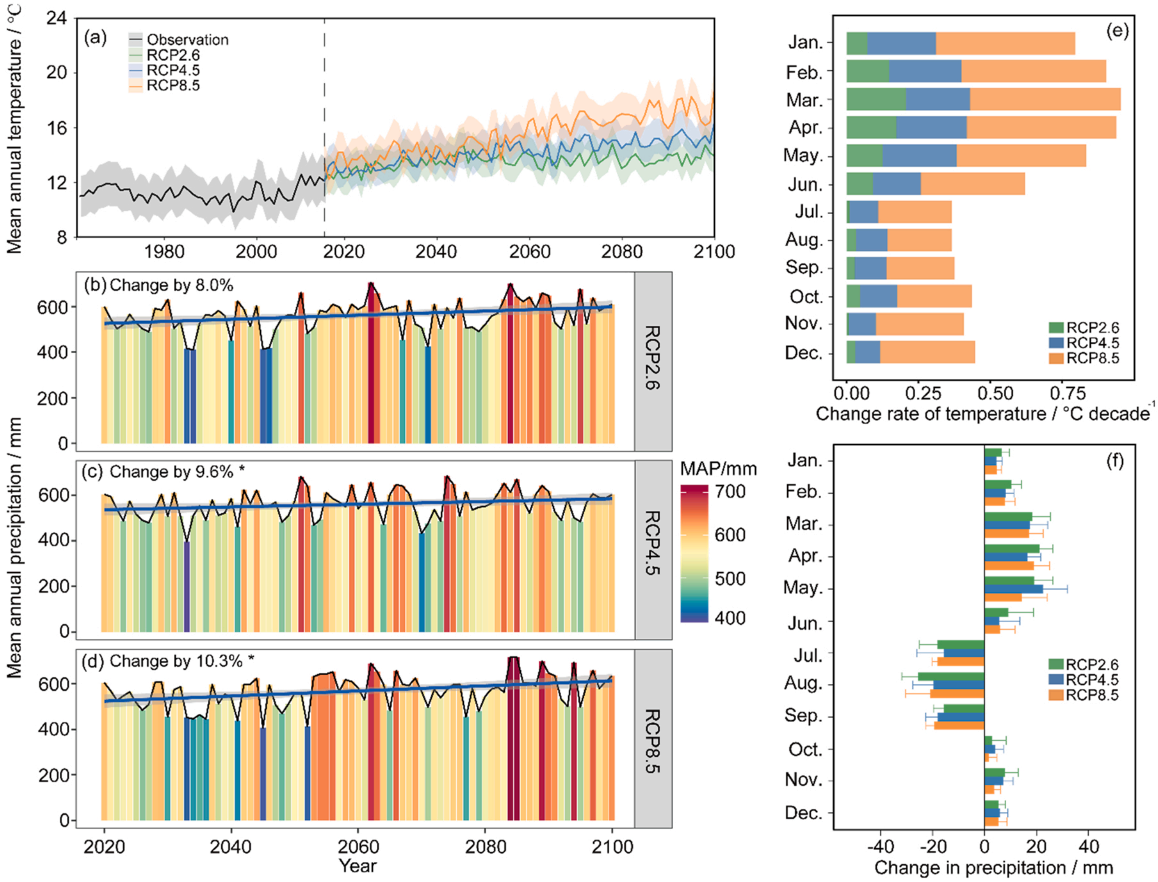

Fig. 5. Projected mean annual temperature (MAT, a), precipitation (MAP, b–d), as well as mean monthly temperature (e) and precipitation variations (f) over the Chaohe watershed under three RCPs compared with the historical period from 1961 to 2015.

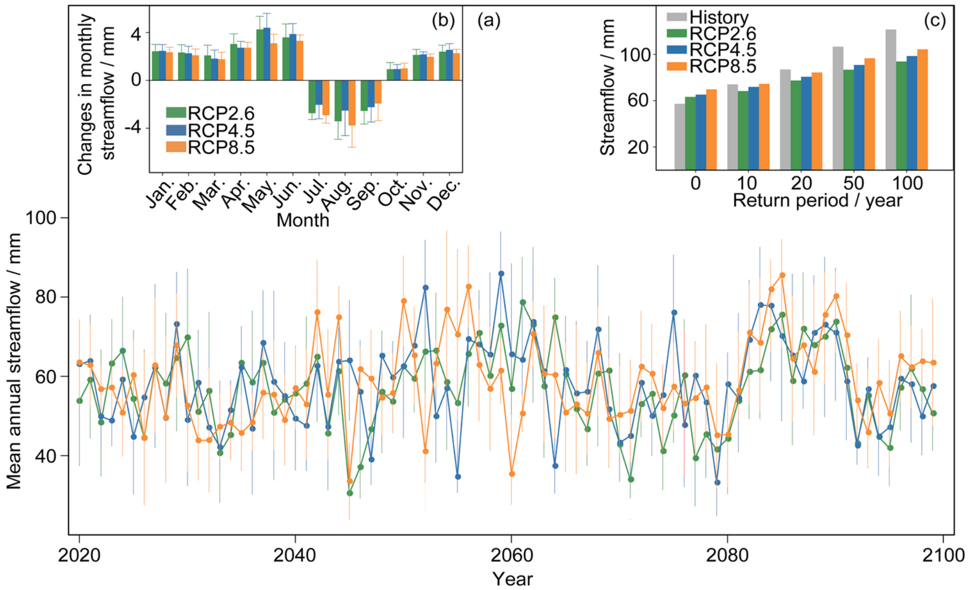

Fig. 6. Predicted mean annual (a), changes in monthly streamflow (b, inserted panel), and return periods of annual streamflow (c, inserted panel) under three emission scenarios from 2020 to 2100.

pathways, respectively. In addition, among the three RCPs, there is an upward trend detected in RCP8.5 and RCP 4.5 scenarios, while there has less variation in the low-level emission scenario.

3.2.2. Monthly temperature and precipitation changes in the future

Global climate change has also altered the intra-annual distribution of precipitation and temperature. The same is true for annual and monthly temperatures that also show notable warming trends, although there are slight differences between the three emission pathways (Fig. 5e). Specifically, mean monthly temperature change is sensitive to radiation forcing and increases with intensifying radiation conditions from scenario RCP2.6 to RCP8.5. As a result, future temperature increases during summer exceed the mean annual change by 1.2 ℃ (RCP8.5), 0.6 ℃ (RCP4.5), and 0.4 ℃ (RCP2.6). In addition, a majority of the future monthly precipitation is higher than the historical level reflected by observed data for the period 1961–2015. Significant differences in intra-annual precipitation variation between the summer monsoon and other seasons are also projected. Although mean annual precipitation is projected to increase (Figs. 5b–d), the precipitation decrease was forecasted in the summer months (i.e., July to September) in the Chaohe watershed (Fig. 5f). Hereinto, the rates of summer precipitation variation were 18.3%, 14.2%, and 13.3% below the low-level, medium-level and high-level emission pathways, respectively, relative to the summer precipitation for the historical period 1961–2015.

3.3. Future streamflow and evapotranspiration change under climate change

3.3.1. Streamflow and evapotranspiration variations at the annual scale

The increasing trend of annual streamflow agrees well with the projected annual precipitation under all three RCPs conditions (Fig. 6a). Hereinto, the increase of annual streamflow is more dramatic under the RCP8.5 scenario (increase by 4.6% compared with the historical period) than that under the medium (3.7%) and low (1.3%) emission scenarios, until the end of the 21st century. Moreover, similar to the annual precipitation variation, there will be a small change in the low and medium emission conditions but a significant upward under the RCP8.5 pathway.

As critical information for risk assessment, streamflow return levels of the historical and future periods are illustrated in Fig. 6c. Under three warming scenarios, the 5-year streamflow return period will increase by 10.5–21.9% ($p < 0.01$) until the end of this century. The streamflow under 20-year, 50-year, or 100-year return scenarios are all projected to decrease ($p < 0.01$). For example, streamflow with the return period of 100 years will decrease by 14.1–22.8%. Conversely, the difference in streamflow with a 10-year return period is insignificant ($p = 0.46$). Moreover, no significant differences are found among the three future climate scenarios with all return period levels ($p = 0.41$). A similar long-term rising trend of annual evapotranspiration (*ET*) will occur among the different RCP pathways from the early 2020 s to the late 2100 s (Fig. 7a). From 2020–2100, the watershed *ET* is expected to increase by 13.1% ($p = 0.25$), 9.6% ($p = 0.12$), and 5.3% ($p = 0.11$) compared with the historical annual average (461.1 mm) under the high, medium and low emission scenarios, respectively.

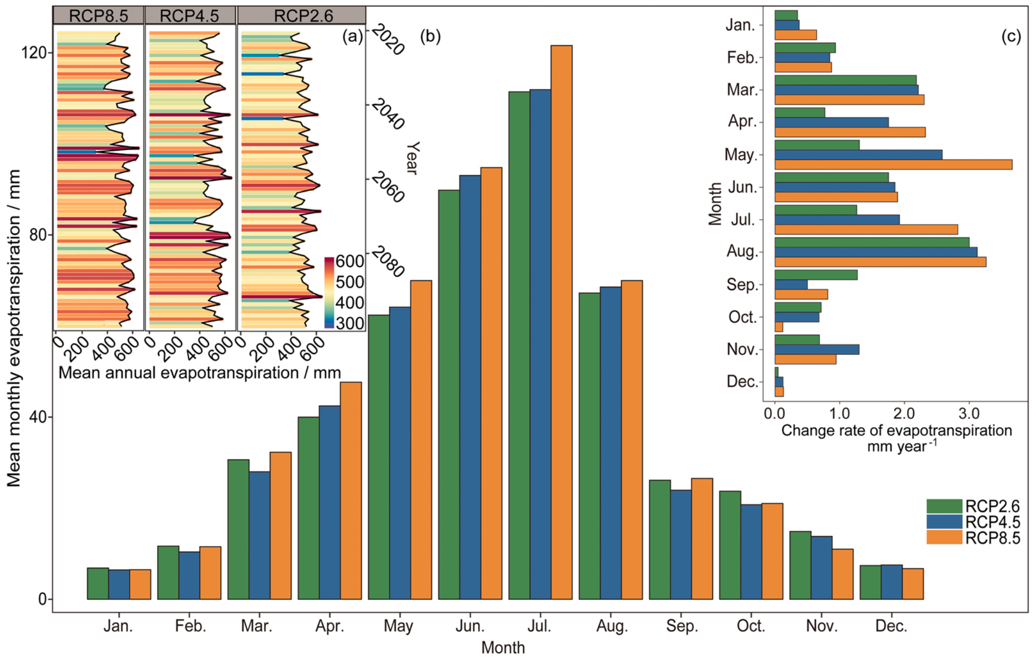

Fig. 7. Mean annual (a, inserted panel) and monthly evapotranspiration (*ET*) changes (b), and the change rate of *ET* (c, inserted panel) under three pathways.

3.3.2. Streamflow and evapotranspiration variations at the seasonal scale

The monthly dispersion coefficient (D_c) of streamflow will increase overall from the historical period under the three RCPs and will be the largest under the high-level emission pathway than the other two scenarios in most months (Fig. 8). Notably, monthly D_c from July to September shows a sizeable increase of up to 200%, manifesting an apparent unstable streamflow variation during the summer monsoon months in the future.

Large differences in streamflow are found between seasons caused by seasonal differences in precipitation and temperature changes (Fig. 6). Mean monthly streamflow projection during 2020–2100 shows the maximum in summer (27.3 mm, 28.4 mm, and 29.1 mm under the scenario RCP2.6, RCP4.5, and RCP8.5, respectively), consistent with the timing of the observed mean monthly streamflow in the historical period. In addition, a negative trend of mean monthly streamflow is projected during the summer monsoon period for all the RCP scenarios by a range of 21.3–30.5% in July, 16.9–31.7% in August, and 28.1–37.0% in September, compared with the historical period, respectively. The streamflow trends are contrary to the increase projected for all other months throughout the year. The seasonal variations in *ET* for three pathways are shown in Fig. 7b. Minimum cumulative *ET* in the winter months from December to February, *ET* is lower than other seasons because of low evaporation demand. Afterwards, *ET* increases gradually due to canopy emergence. Monthly *ET* exhibits a single peak at the watershed per year with the maximum value appeared in July (113.2–124.1 mm under the three RCPs). In spring and autumn, the cumulative *ET* ranges from 130.5 to 145.3 mm, and 58.5–64.7 mm under the scenario RCP2.6, RCP4.5, and RCP8.5, respectively (Fig. 7b). Additionally, the distribution of the change rate (*CR*, mm per year) of monthly *ET* differs under the three RCPs. The positive monthly *ET* trend is consistent with the expected acceleration of the hydrological cycle caused by an increased evaporative demand associated with rising radiative forcing and temperatures (Fig. 7c). For instance, a relatively high *CR* of *ET* from the early 2020 s to the late 2090 s in summer has the values of 5.5 mm, 6.3 mm, and 6.9 mm per year without a significant variation under low, medium, and high emission scenarios, respectively.

Fig. 9 depicts the relationships between streamflow and precipitation variations at monthly and annual scales under the three RCPs from 2020 to 2100, respectively. Overall, the correlation coefficients between monthly streamflow and monthly precipitation are 0.91 (in RCP2.6, $p < 0.001$), 0.86 (in RCP4.5, $p < 0.001$), and 0.89 (in RCP8.5, $p < 0.001$), which indicate the monthly streamflow change under all the RCPs scenarios corresponds to the precipitation variation very well (Fig. 9a). Annual streamflow and precipitation variations are significantly correlated (i.e., correlation coefficients 0.77, 0.72. and 0.67 under three pathways, respectively, $p < 0.001$, Fig. 9b). Correlation coefficients between summer streamflow and precipitation variations are as high as 0.99 under the RCP4.5 ($p < 0.01$, Fig. 9c) and 0.76 under the RCP2.6 ($p < 0.01$, Fig. 9c). The correlation coefficients between non-summer streamflow variations and the monthly precipitation fluctuations are significant (Fig. 9d, $p < 0.001$ and $p < 0.01$ under the RCP2.6, the RCP4.5, and the RC8.5, respectively).

4. Discussion

4.1. Climate differences between summer monsoon and other seasons

Projected annual precipitation and temperature under all the emission scenarios indicated that the watershed is likely to be wetter and warmer until the end of this century. The projected future temperature for the watershed will increase by 0.8–3.8 °C by 2100 under the three representative concentration pathways in line with the projected future warming over China, particularly in northern China, and an even more significant warming trend compared with the annual mean temperature increase by 0.4–1.3 °C per century from 1906 to 2005 (Chen and Frauenfeld, 2014; Wu and Ma, 2012). In northern China, the warming and its consequences for the water cycle are related to the northwards shift of climate zones (Litschi et al., 2006). Although there is some inter-annual and decadal fluctuation, the wetting trend is consistent with most global model predictions (Alfieri et al., 2015; Aloysius and Saiers, 2017).

Decreased precipitation forecasted in this watershed during the summer monsoon period, (contrary to other seasons), is mainly

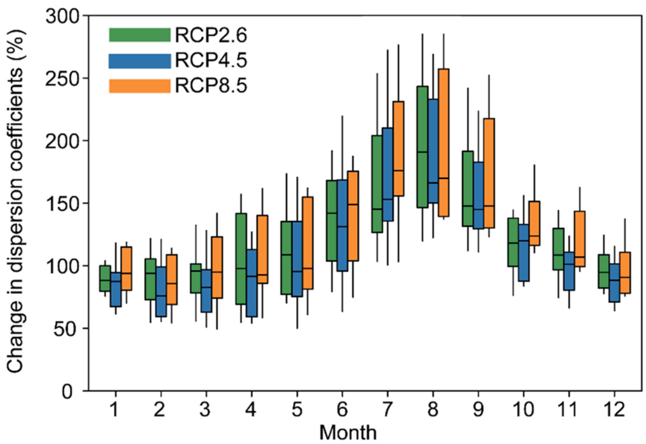

Fig. 8. Changes in future dispersion coefficient (*Dc*) of monthly streamflow from the historical period (1961–2015).

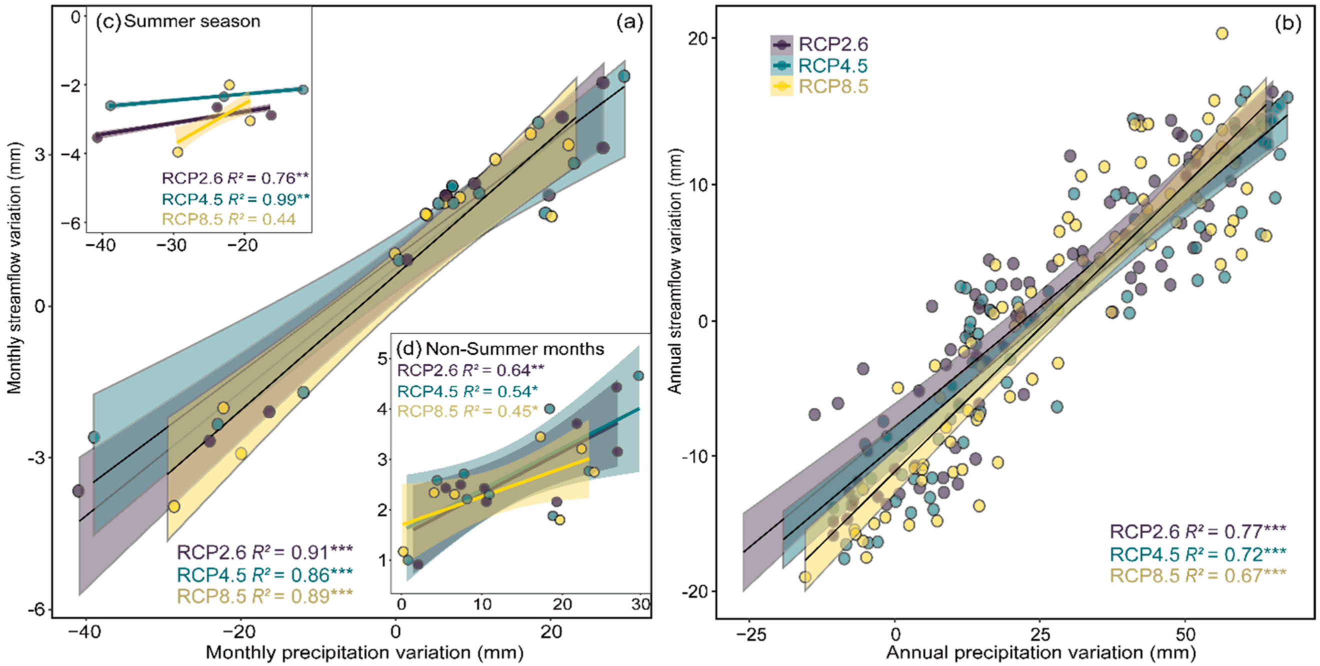

Fig. 9. Changes in streamflow against the variations in precipitation at monthly (a) and annual scales (b), and for summer months (c, inserted panel in (a)) and non-summer months (d, inserted panel in (a)) under three RCPs during 2020–2100 (*, **, and *** mean significant at $p < 0.05$, $p < 0.01$ and $p < 0.001$, respectively).

driven by a weakening of the EASM. In northern China, the EASM delivers around 60–70% of yearly precipitation (Lei et al., 2010). Reduced sea-surface temperature gradients hinder the Asian summer monsoon, thus preventing ocean moisture from reaching northern China (Jiang et al., 2017). Moreover, El Niño's strongly impact on summer precipitation is also responsible for the northern China droughts (Ouyang et al., 2014). Summer precipitation in northern China might be reduced by up to 30% in reaction to a 1 °C El Niño sea surface temperature anomaly (Wen et al., 2015). Beyond that, other reasons such as surface cooling caused by aerosol forcing also facilitate the weakening of the EASM (Song et al., 2014).

4.2. Changes in annual streamflow characteristics

Precipitation is fundamental for the sustainable development of terrestrial ecosystems. As a vital natural water resource, precipitation influences streamflow directly, while evapotranspiration is also constrained by other environmental factors such as temperature, humidity, and radiation (Qi et al., 2019). Previous studies indicated that the precipitation changes are the dominant cause of streamflow variations (Zhang et al., 2011). A strong positive correlation ($p < 0.001$) existed between precipitation and streamflow over this water-limited watershed at both annual and monthly scales (Fig. 9), and increasing precipitation provides more available water. Besides the water supply, increasing evapotranspiration caused by surface warming is also a critical driver of streamflow variation and drought risk prediction. Evapotranspiration affects streamflow similarly in different seasons, though having different magnitudes. The positive *ET* variation trend, until 2100, is expected to increase by 13.1%, 9.6%, and 5.3% compared with the historical annual average (461.1 mm) under high, medium, and low emission scenarios, respectively. Previous studies also verified a persistent increase in evapotranspiration over China for both target warming scenarios (Yao et al., 2020; Zhang et al., 2018). Hereinto, the positive changes in evapotranspiration are more significant for the 2.0 °C warming in the parts of northern China than those at the 1.5 °C warming (Su et al., 2018). Meanwhile, significant increases in potential evapotranspiration are also projected throughout China for both target periods. The percentage increase in precipitation averaged over land is around 1.7% per degree Celsius rise in mean surface air temperature, while the increase in potential evapotranspiration is 5.3% per degree Celsius (Fu and Feng, 2014).

It is vital to weigh the increasing precipitation and the intensifying water consumption under climate warming. Studied suggested that, under the 1.5 °C global warming scenario, increasing trends of evapotranspiration and precipitation are projected across China. The scenario also suggests a trend toward wetter conditions in north China caused by a more substantial impact of increases in precipitation than in evapotranspiration (Su et al., 2018). Nevertheless, the opposite tendency is also found in arid northwestern China caused by high evapotranspiration. The rate of *ET* increases would be two or three times larger than that of precipitation at the end of the 21st century (Yao et al., 2019). Moreover, soil moisture and groundwater recharge are likely to decrease due to the warming-induced increase in vapor pressure deficit and the increase in evaporative demand of the atmosphere (i.e., potential evapotranspiration) (Berg and Sheffield, 2018). These changes will substantially impact the terrestrial ecosystem structure and function (Xu et al., 2019; Zhu et al., 2020).

4.3. Changes in seasonal streamflow characteristics

As climate variability primarily refers, the variations in air temperature and precipitation control the response of the watershed's flow to changing climate (Yang et al., 2014). And studies across China did exhibit this response, and also projected that varied hydrological responses of seasonal climate change patterns (Shi et al., 2007; Zhang et al., 2011). Streamflow from October to February increases in all RCPs due to the combined effects of increasing precipitation in winter and low evapotranspiration demand (Figs. 5f and 6b). Consistent with other studies that increasing streamflow is mainly caused by the combined effects of increasing precipitation in winter and spring, and therefore warmer watersheds that experience flood events throughout this period are predominately projected to show increases in peak monthly flow (Byun et al., 2019). While, higher evapotranspiration stimulated by rising temperature (Fig. 5e) with declining precipitation (Fig. 5f) contributed substantially to the streamflow decreased during the summer monsoon season (Fig. 6). Although the higher available water for plants could mitigate the effects of higher temperatures to some extent, because of diminished precipitation and subsequent reductions in available water will limit the response of *ET* at the watershed to increases in air temperature. Diminished precipitation during the growing season increases water stress on vegetation and decreases the photosynthetic rate, which causes a decrease in *ET* (Pourmokhtarian et al., 2017). Therefore, reduced available moisture supply and drought risks driven by a warmer and drier summer climate would negatively affect vegetation and further increase the carbon emission for terrestrial ecosystems. Undoubtedly, streamflow fluctuation caused by climate change poses more difficult challenges to dealing with extreme hydrological events and watershed ecosystem management (Rana et al., 2014). On the positive side, increased precipitation in spring, fall, and winter would reduce the drought risks and provide more available water for terrestrial vegetation (Gherardi and Sala, 2015).

In addition, alterations in the magnitude of characteristic flows identify potential threats from global warming and have critical implications for future water resource management (Soriano et al., 2020; Yazdandoost et al., 2020). An upward trend in the annual streamflow with a short-term return period is projected under all scenarios (Fig. 6c). Increased precipitation across the watershed could favor mitigation of water scarcity and drought in the water-limited regions during the non-summer monsoon months (Fig. 5f). While the opposite trend is also revealed in parts of northern China, where may experience warmer annual temperatures, and have drier springs and early summers (March–June) under 1.5 and 2 °C global warming (Liu et al., 2017). Moreover, streamflow with long-term return periods, such as 20-year, 50-year, or 100-year return levels, is expected to decrease in the future (Fig. 6c). To some extent, the study catchment may benefit from the warming environment during the drier summers to early autumns (July–September), which would potentially lead to fewer floods during the rainy season. Consequently, it is critical to establish appropriate adaptation strategies to mitigate climate change's adverse effects on streamflow and increase watershed resilience to extreme climate events (Hongxing et al., 2007).

One of the critical challenges in assessing the effects of climate change on the hydrological regimes is determining how vegetation changes with increasing carbon dioxide concentration and variations in precipitation and temperature (Novick et al., 2016) because ecological processes are inextricably linked to hydrological processes and both of which are subject to climate change (Jiao et al., 2017). Specifically, changes in ecological processes regulate hydrological processes (e.g., streamflow and infiltration) through altering precipitation interception, interception/soil evaporation, and plant transpiration (Asbjornsen et al., 2011). Therefore, future climate change can indirectly modulate hydrological regimes by affecting vegetation dynamics. Vegetation growth induced by increasing carbon dioxide concentration will consume more available water through transpiration in the future, resulting in local streamflow reduction, despite the fact that they accelerate the water cycle at a large scale (Hunt et al., 2020; Sun et al., 2020). Future studies should focus on incorporating and quantifying the interactions and feedbacks among climate change, vegetation dynamics, and hydrological regimes.

5. Conclusions

Variations in climate and streamflow in the future at annual and seasonal scales are forecasted for the most critical drinking water reservoir watershed for metropolitan Beijing, located in the temperate monsoon climate region of northern China. Overall, the watershed is likely to become warmer and wetter while the summer monsoon period experiences a drier and warmer trend until the end of this century. Consequently, future monthly streamflow during the summer will decrease due to reduced precipitation and increased evapotranspiration while increasing in other seasons. Moreover, climate change also affects watershed water resources and extreme hydrological events. On one hand, the predicted increase in the short-term return period annual streamflow could ease the water shortage and reduce the drought risks in the non-summer monsoon seasons. On the other hand, the projected variations in streamflow with return periods of 20-year, 50-year, or 100-year will be reduced due to the decrease in summer precipitation, which could reduce flood risks during the summer monsoon period.

CRediT authorship contribution statement

Wenxu Cao: Conceptualization, Writing – original draft, Methodology, Formal analysis, **Zhiqiang Zhang:** Conceptualization, Data curation, Supervision, Writing – review & editing, **Yongqiang Liu:** Writing – review & editing, **Lawrence E. Band:** Writing – review & editing, **Shengping Wang:** Writing – review & editing, **Hang Xu:** Writing – review & editing.

Declaration of Competing Interest

The authors declare that they have no known competing financial interests or personal relationships that could have appeared to influence the work reported in this paper.

Acknowledgments

This study was financially supported by the National Key Research and Development Program of China (2017YFE0118100), the National Natural Science Foundation of China (Grant No. 41140011) and the Beijing Municipal Education Committee for Interdisciplinary Program Ecological Restoration Engineering. We acknowledge the Hydrology and Water Resource Survey Bureau of Hebei Province, Beijing Water Authority and Haihe River Water Conservancy Commission for providing climate and hydrological data. The first author also acknowledges the support from Beijing Municipal Education Committee through a postgraduate training program entitled "Effect of forest vegetation restoration on hydrology in the upper reaches of Miyun Reservoir''. Finally, all authors acknowledge anonymous reviewers and the handling editor for their constructive and insightful comments and suggestions, significantly improving the final version. Meanwhile, the authors also thank Dr. Steven G. McNulty, Research Scientist of USDA Forest Service for his linguistic assistance to revise this manuscript.

Appendix A. Supporting information

Supplementary data associated with this article can be found in the online version at doi:10.1016/j.ejrh.2021.100959.

References

Ahmadalipour, A., Rana, A., Moradkhani, H., Sharma, A., 2017. Multi-criteria evaluation of CMIP5 GCMs for climate change impact analysis. Theor. Appl. Climatol. 128, 71–87. https://doi.org/10.1007/s00704-015-1695-4.

Alfieri, L., Burek, P., Feyen, L., Forzieri, G., 2015. Global warming increases the frequency of river floods in Europe. Hydrol. Earth Syst. Sci. 19, 2247–2260. https://doi.org/10.5194/hess-19-2247-2015.

Aloysius, N., Saiers, J., 2017. Simulated hydrologic response to projected changes in precipitation and temperature in the Congo River basin. Hydrol. Earth Syst. Sci. 21, 4115–4130. https://doi.org/10.5194/hess-21-4115-2017.

Asbjornsen, H., Goldsmith, G.R., Alvarado-Barrientos, M.S., Rebel, K., Van Osch, F.P., Rietkerk, M., Chen, J., Gotsch, S., Tobón, C., Geissert, D.R., Gómez-Tagle, A., Vache, K., Dawson, T.E., 2011. Ecohydrological advances and applications in plant-water relations research: a review. J. Plant Ecol. 4, 3–22. https://doi.org/10.1093/jpe/rtr005.

Asseng, S., Ewert, F., Rosenzweig, C., Jones, J.W., Hatfield, J.L., Ruane, A.C., Boote, K.J., Thorburn, P.J., Rötter, R.P., Cammarano, D., Brisson, N., Basso, B., Martre, P., Aggarwal, P.K., Angulo, C., Bertuzzi, P., Biernath, C., Challinor, A.J., Doltra, J., Gayler, S., Goldberg, R., Grant, R., Heng, L., Hooker, J., Hunt, L.A., Ingwersen, J., Izaurralde, R.C., Kersebaum, K.C., Müller, C., Naresh Kumar, S., Nendel, C., O'Leary, G., Olesen, J.E., Osborne, T.M., Palosuo, T., Priesack, E., Ripoche, D., Semenov, M.A., Shcherbak, I., Steduto, P., Stöckle, C., Stratonovitch, P., Streck, T., Supit, I., Tao, F., Travasso, M., Waha, K., Wallach, D., White, J.W., Williams, J.R., Wolf, J., 2013. Uncertainty in simulating wheat yields under climate change. Nat. Clim. Chang. 3, 827–832. https://doi.org/10.1038/nclimate1916.

Band, L.E., Mackay, D.S., Creed, I.F., Semkin, R., Jeffries, D., 1996. Ecosystem processes at the watershed scale: sensitivity to potential climate change Ray Semkin and Deah Jeflies. Limnol. Oceanogr. 41, 928–938.

Band, L.E., Tague, C.L., Brun, S.E., Tenenbaum, D.E., Fernandes, R. a, 2000. Modelling watersheds as spatial object hierarchies: structure and dynamics. Trans. GIS 4, 181–196. https://doi.org/10.1111/1467-9671.00048.

Berg, A., Sheffield, J., 2018. Climate Change and Drought: the Soil Moisture Perspective. Curr. Clim. Chang. reportsorts 4, 180–191.

Blöschl, G., Hall, J., Viglione, A., Perdigão, R.A.P., Parajka, J., Merz, B., Lun, D., Arheimer, B., Aronica, G.T., Bilibashi, A., Boháč, M., Bonacci, O., Borga, M., Čanjevac, I., Castellarin, A., Chirico, G.B., Claps, P., Frolova, N., Ganora, D., Gorbachova, L., Gül, A., Hannaford, J., Harrigan, S., Kireeva, M., Kiss, A., Kjeldsen, T. R., Kohnová, S., Koskela, J.J., Ledvinka, O., Macdonald, N., Mavrova-Guirguinova, M., Mediero, L., Merz, R., Molnar, P., Montanari, A., Murphy, C., Osuch, M., Ovcharuk, V., Radevski, I., Salinas, J.L., Sauquet, E., Šraj, M., Szolgay, J., Volpi, E., Wilson, D., Zaimi, K., Živković, N., 2019. Changing climate both increases and decreases European river floods. Nature 573, 108–111. https://doi.org/10.1038/s41586-019-1495-6.

Byun, K., Chiu, C.M., Hamlet, A.F., 2019. Effects of 21st century climate change on seasonal flow regimes and hydrologic extremes over the Midwest and Great Lakes region of the US. Sci. Total Environ. 650, 1261–1277. https://doi.org/10.1016/j.scitotenv.2018.09.063.

Cao, W., Zhiqiang, Z., Tonggang, Z., Shengping, W., Guo, Junting, Xu, Hang, 2018. Explornig the effects of vegetation dynamics and climate changes on the Chaohe watershed actual evapotranspiration-Budyko Hypothesis approach. Acta Ecol. Sin. 38.

Chen, L., Frauenfeld, O.W., 2014. Surface air temperature changes over the twentieth and twenty-first centuries in China simulated by 20 CMIP5 models. J. Clim. 27, 3920–3937. https://doi.org/10.1175/JCLI-D-13-00465.1.

Dai, A., Qian, T., Trenberth, K.E., Milliman, J.D., 2009. Changes in continental freshwater discharge from 1948-2004. J. Clim. 22, 2773–2792.

Donat, M.G., Lowry, A.L., Alexander, L.V., Gorman, P.A.O., Maher, N., 2016. More extreme precipitation in the world ' s dry and wet regions. Nat. Clim. Change 6, 508–513. https://doi.org/10.1038/NCLIMATE2941.

Fatichi, S., Vivoni, E.R., Ogden, F.L., Ivanov, V.Y., Mirus, B., Gochis, D., Downer, C.W., Camporese, M., Davison, J.H., Ebel, B., Jones, N., Kim, J., Mascaro, G., Niswonger, R., Restrepo, P., Rigon, R., Shen, C., Sulis, M., Tarboton, D., 2016. An overview of current applications, challenges, and future trends in distributed process-based models in hydrology. J. Hydrol. 537, 45–60. https://doi.org/10.1016/j.jhydrol.2016.03.026.

Fu, Q., Feng, S., 2014. Responses of terrestrial aridity to global warming. J. Geophys. Res. Atmos. 119, 7863–7875. https://doi.org/10.1002/2014JD021608.Received.

Getachew, B., Manjunatha, B.R., Bhat, H.G., 2021. Modeling projected impacts of climate and land use/land cover changes on hydrological responses in the Lake Tana Basin, upper Blue Nile River Basin, Ethiopia. J. Hydrol. 595, 125974 https://doi.org/10.1016/j.jhydrol.2021.125974.

Gherardi, L.A., Sala, O.E., 2015. Enhanced precipitation variability decreases grass- and increases shrub-productivity. Proc. Natl. Acad. Sci. U.S.A. 112, 12735–12740. https://doi.org/10.1073/pnas.1506433112.

Gizaw, M.S., Biftu, G.F., Gan, T.Y., Moges, S.A., 2017. Potential impact of climate change on streamflow of major Ethiopian rivers. Clim. Chang. 143, 371–383. https://doi.org/10.1007/s10584-017-2021-1.

Hargreaves, J.C., 2010. Skill and uncertainty in climate models. Wiley Interdiscip. Rev. Clim. Chang. 1, 556–564. https://doi.org/10.1002/wcc.58.

He, W. ping, Zhao, S. shan, Wu, Q., Jiang, Y. di, Wan, S., 2019. Simulating evaluation and projection of the climate zones over China by CMIP5 models. Clim. Dyn. 52, 2597–2612. https://doi.org/10.1007/s00382-018-4410-1.

Hirabayashi, Y., Mahendran, R., Koirala, S., Konoshima, L., Yamazaki, D., Hirabayashi, Y., Mahendran, R., Koirala, S., Konoshima, L., 2013. Global flood risk under climate change. Nat. Clim. Chang. 3, 816–821. https://doi.org/10.1038/NCLIMATE1911.

Hongxing, Z., Lu, Z., Changming, L., Quanxi, S., Yoshihiro, F., 2007. Changes in stream flow regime in headwater catchments of the Yellow River basin since the 1950s. Hydrol. Process 886–893. https://doi.org/10.1002/hyp.6280.

Hunt, J.R., Celestina, C., Kirkegaard, J.A., 2020. The realities of climate change, conservation agriculture and soil carbon sequestration. Glob. Chang. Biol. 26, 3188–3189. https://doi.org/10.1111/gcb.15082.

Jarvis, P.G., 1976. The interpretation of the variations in leaf water potential and stomatal conductance found in canopies in the field. Philos. Soc. R. Soc. Lond. Ser. B Biol. Sci. 273 (927), 593–610. https://doi.org/10.1098/rstb.1976.0035.

Jiang, Z., Jiang, S., Shi, Y., Liu, Z., Li, W., Li, L., 2017. Impact of moisture source variation on decadal-scale changes of precipitation in North China from 1951 to 2010. J. Geophys. Res. Atmos. 12, 600–613. https://doi.org/10.1002/2016JD025795.

Jiao, Y., Lei, H., Yang, D., Huang, M., Liu, D., Yuan, X., 2017. Impact of vegetation dynamics on hydrological processes in a semi-arid basin by using a land surface-hydrology coupled model. J. Hydrol. 551, 116–131. https://doi.org/10.1016/j.jhydrol.2017.05.060.

Kite, G.W., Dalton, A., Dion, K., 1994. Simulation of streamflow in a macroscale watershed using general circulation model data. Water Resour. Res. 30, 1547–1559.

Legates, Mccabe, 1999. Evaluating the Use Of " Goodness-of-Fit " Measures in Hydrologic and Hydroclimatic Model Validation Evaluating the use of " goodness-of-fit " measures in hydrologic and hydroclimatic model validation. Water Resour. Res. 35, 233–241. https://doi.org/10.1029/1998WR900018.

Lei, Y., Hoskins, B., Slingo, J., 2010. Exploring the Interplay between Natural Decadal Variability and Anthropogenic Climate Change in Summer Rainfall over China. Part I: observational evidence. J. Clim. 24, 4584–4599. https://doi.org/10.1175/2010JCLI3794.1.

Li, Z., Li, X., Xu, Z., 2010. Impacts of water conservancy and soil conservation measures on annual runoff in the Chaohe River Basin during 1961-2005. J. Geogr. Sci. 20, 947–960. https://doi.org/10.1007/s11442-010-0823-4.

Litschi, M., Scha, C., Seneviratne, S.I., Lu, D., 2006. Land – atmosphere coupling and climate change in Europe. Nature 443, 205–209 doi:10.1038/nature0509. ⟨https://doi.org/10.1038/nature05095⟩.

Liu, L., Xu, H., Wang, Y., Jiang, T., 2017. Impacts of 1.5 and 2°C global warming on water availability and extreme hydrological events in Yiluo and Beijiang River catchments in China. Clim. Change 145, 145–158. https://doi.org/10.1007/s10584-017-2072-3.

Liu Y.Q., Goodrick S., Stanturf J.A., 2021, Climate downscaling for fire management, in "Sustainability in Natural Resources Management and Land Planning", World Sustainability Series, https://doi.org/10.1007/978–3-030–76624-5–27.

López-Ballesteros, A., Senent-Aparicio, J., Martínez, C., Pérez-Sánchez, J., 2020. Assessment of future hydrologic alteration due to climate change in the Aracthos River basin (NW Greece). Sci. Total Environ. 733, 139299 https://doi.org/10.1016/j.scitotenv.2020.139299.

Lou, J., Zhiqiang, Z., Junting, G., Yangxu, Y., Ankun, Y., Tiezhang, H., 2015. Impact of landscape pattern change on runoff in chaohe river watershed. Bull. Soil Water Conserv. 35, 34–39. https://doi.org/10.13961/j.cnki.stbctb.2015.04.008.

Lutz, A.F., ter Maat, H.W., Biemans, H., Shrestha, A.B., Wester, P., Immerzeel, W.W., 2016. Selecting representative climate models for climate change impact studies: an advanced envelope-based selection approach. Int. J. Climatol. 36, 3988–4005. https://doi.org/10.1002/joc.4608.

Moriasi, D., Arnold, J., Liew, M.W. Van, 2013. Model Evaluation Guidelines for Systematic Quantification of Accuracy in Watershed Simulations. https://doi.org/10.13031/2013.23153.

Moss, R.H., Edmonds, J.A., Hibbard, K.A., Manning, M.R., Rose, S.K., Vuuren, D.P., Van, Carter, T.R., Emori, S., Kainuma, M., Kram, T., Meehl, G.A., Mitchell, J.F.B., Nakicenovic, N., Riahi, K., Smith, S.J., Stouffer, R.J., Thomson, A.M., Weyant, J.P., Wilbanks, T.J., 2010. The next generation of scenarios for climate change research and assessment. Nature 463, 747–756. https://doi.org/10.1038/nature08823.

Nash, E., Sutcliffe, V., 1970. Part i- a discussion of principles 10, 282–290.

Novick, K.A., Ficklin, D.L., Stoy, P.C., Williams, C.A., Bohrer, G., Oishi, A.C., Papuga, S.A., Blanken, P.D., Noormets, A., Sulman, B.N., Scott, R.L., Wang, L., Phillips, R.P., 2016. The increasing importance of atmospheric demand for ecosystem water and carbon fluxes. Nat. Clim. Chang. 6, 1023–1027. https://doi.org/10.1038/nclimate3114.

O'Callaghan, J.F., Mark, D.M., 1984. The extraction of ordered vector drainage networks from elevation data. Comput. Vision Graph. Image Process. 28, 323–344. https://doi.org/10.1016/0734-189X(89)90053-4.

Ouyang, F., Zhu, Y., Fu, G., Lü, H., Zhang, A., Yu, Z., Chen, X., 2015. Impacts of climate change under CMIP5 RCP scenarios on streamflow in the Huangnizhuang catchment. Stoch. Environ. Res. Risk Assess. 29, 1781–1795. https://doi.org/10.1007/s00477-014-1018-9.

Ouyang, R., Liu, W., Fu, G., Liu, C., Hu, L., Wang, H., 2014. Linkages between ENSO / PDO signals and precipitation, streamflow in China during the last 100 years. Hydrol. Earth Syst. Sci. 18, 3651–3661. https://doi.org/10.5194/hess-18-3651-2014.

Philip, J.T., 1957. The Theory of Infiltration: 4. Sorptivity and Algebraic Infiltration Equations. 877Soil Science. 84 (3) 257–264. doi:10.1097/00010694–195709000-0001.

Piao, S., Ciais, P., Huang, Y., Shen, Z., Peng, S., Li, J., Zhou, L., Liu, H., Ma, Y., Ding, Y., Friedlingstein, P., Liu, C., Tan, K., Yu, Y., Zhang, T., Fang, J., 2010. The impacts of climate change on water resources and agriculture in China. Nature 467, 43–51. https://doi.org/10.1038/nature09364.

Pourmokhtarian, A., Driscoll, C.T., Campbell, J.L., Hayhoe, K., Stoner, A.M.K., Adams, M.B., Burns, D., Fernandez, I., Mitchell, M.J., Shanley, J.B., 2017. Modeled ecohydrological responses to climate change at seven small watersheds in the northeastern United States. Glob. Chang. Biol. 23, 840–856. https://doi.org/10.1111/gcb.13444.

Qi, W., Liu, J., Leung, F., 2019. A framework to quantify impacts of elevated CO 2 concentration, global warming and leaf area changes on seasonal variations of water resources on a river basin scale. J. Hydrol. 570, 508–522. https://doi.org/10.1016/j.jhydrol.2019.01.015.

Rana, A., Foster, K., Bosshard, T., Olsson, J., Bengtsson, L., 2014. Impact of climate change on rainfall over Mumbai using distribution-based scaling of global climate model projections. J. Hydrol. Reg. Stud. 1, 107–128. https://doi.org/10.1016/j.ejrh.2014.06.005.

Reynolds, L.V., Shafroth, P.B., Poff, N.L., 2015. Modeled intermittency risk for small streams in the Upper Colorado River Basin under climate change. J. Hydrol. 523, 768–780. https://doi.org/10.1016/j.jhydrol.2015.02.025.

Seddon, A.W.R., Macias-fauria, M., Long, P.R., Benz, D., Willis, K.J., 2016. Sensitivity of global terrestrial ecosystems to climate variability. Nature 531, 229–232. https://doi.org/10.1038/nature16986.

Shen, Yan-jun, Shen, Yanjun, Fink, M., Kralisch, S., Chen, Y., Brenning, A., 2018. Trends and variability in streamflow and snowmelt runoff timing in the southern Tianshan Mountains. J. Hydrol. 557, 173–181. https://doi.org/10.1016/j.jhydrol.2017.12.035.

Shi, Y., Shen, Y., Kang, E., Li, D., Ding, Y., Zhang, G., Hu, R., 2007. Recent and future climate change in northwest China. Clim. Change 80, 379–393. https://doi.org/10.1007/s10584-006-9121-7.

Song, F., Northwest, P., Zhou, T., 2014. Responses of East Asian summer monsoon to natural and anthropogenic forcings in the 17 latest CMIP5 models. Geophys. Res. Lett. 41, 596–603. https://doi.org/10.1002/2013GL058705.

Soriano, E., Mediero, L., Garijo, C., 2020. Quantification of expected changes in peak flow quantiles in climate change by combining continuous hydrological modelling with the modified curve number method. Water Resour. Manag. 34, 4381–4397. https://doi.org/10.1007/s11269-020-02670-w.

Su, B., Huang, J., Fischer, T., Wang, Y., Kundzewicz, Z.W., Zhai, J., Sun, H., Wang, A., Zeng, X., Wang, G., Tao, H., Gemmer, M., Li, X., Jiang, T., 2018. Drought losses in China might double between the 1.5°C and 2.0°C warming. Proc. Natl. Acad. Sci. U.S.A. 115, 10600–10605. https://doi.org/10.1073/pnas.1802129115.

Sun, W., Canadell, J.G., Yu, Lijun, Yu, Lingfei, Zhang, W., Smith, P., Fischer, T., Huang, Y., 2020. Climate drives global soil carbon sequestration and crop yield changes under conservation agriculture. Glob. Chang. Biol. 3325–3335. https://doi.org/10.1111/gcb.15001.

Tague, C., Grant, G., Farrell, M., Choate, J., Jefferson, A., 2008. Deep groundwater mediates streamflow response to climate warming in the Oregon Cascades. Clim. Change 86, 189–210. https://doi.org/10.1007/s10584-007-9294-8.

Tague, C., McMichael, C., Hope, A., Choate, J., Clark, R., 2004. Application of the RHESSys model to a California semiarid shrubland watershed. J. Am. Water Resour. Assoc. 40, 575–589. https://doi.org/10.1111/j.1752-1688.2004.tb04444.x.

Tague, C.L., Band, L.E., 2004. Regional Hydro-ecologic simulation system: An object-oriented approach to spatially distributed modeling of carbon, water and nutrient cycling. Earth Interact. 8, 1–42 (ST-Regional Hydro-ecologic simulation syst).

Tang, L., Yang, D., Hu, H., Gao, B., 2011. Detecting the effect of land-use change on streamflow, sediment and nutrient losses by distributed hydrological simulation. J. Hydrol. 409, 172–182. https://doi.org/10.1016/j.jhydrol.2011.08.015.

Tegegne, G., Park, D.K., Kim, Y.O., 2017. Comparison of hydrological models for the assessment of water resources in a data-scarce region, the Upper Blue Nile River Basin. J. Hydrol. Reg. Stud. 14, 49–66. https://doi.org/10.1016/j.ejrh.2017.10.002.

Thiessen, 1911. Precipitation averages for large areas. Mon. Weather Rev. 39, 1082–1089.

Tong, K., Su, F., Yang, D., Hao, Z., 2014. Evaluation of satellite precipitation retrievals and their potential utilities in hydrologic modeling over the Tibetan Plateau. J. Hydrol. 519, 423–437. https://doi.org/10.1016/j.jhydrol.2014.07.044.

Wang, S., Zhang, Z., Mcvicar, T.R., Guo, J., Tang, Y., Yao, A., 2013. Isolating the impacts of climate change and land use change on decadal streamflow variation: assessing three complementary approaches. J. Hydrol. 507, 63–74. https://doi.org/10.1016/j.jhydrol.2013.10.018.

Wen, N., Liu, Z., Liu, Y., 2015. Direct impact of El Niño on East Asian summer precipitation in the observation. Clim. Dyn. 44, 2979–2987. https://doi.org/10.1007/s00382-015-2605-2.

Wilby, R.L., 2002. SDSM — a decision support tool for the assessment of regional climate change impacts. Environ. Model. Softw. 17, 147–159.

Wilby, R.L., Wigley, T.M.L., 1997. Downscaling general circuation model output: a review of methods and limitations. Prog. Phys. Geogr. 21, 530–548. https://doi.org/10.1177/030913339702100403.

Wu, Z., Ma, T., 2012. How does coldwave frequency in China respond to a warming climate. Clim. Dyn. 39, 2487–2496. https://doi.org/10.1007/s00382-012-1354-8.

Xu, B., Arain, M.A., Black, T.A., Law, B.E., Pastorello, G.Z., 2019. Seasonal variability of forest sensitivity to heat and drought stresses: a synthesis based on carbon fluxes from North American forest ecosystems. Glob. Chang. Biol 00, 1–18. https://doi.org/10.1111/gcb.14843.

Xu, C.Y., Singh, V.P., 2004. Review on regional water resources assessment models under stationary and changing climate. Water Resour. Manag. 18, 591–612. https://doi.org/10.1007/s11269-004-9130-0.

Xu, H., Wang, X., Zhao, C., Yang, X., 2018. . Agricultural and Forest Meteorology Diverse responses of vegetation growth to meteorological drought across climate zones and land biomes in northern China from 1981 to 2014. Agric. For. Meteorol 262, 1–13. https://doi.org/10.1016/j.agrformet.2018.06.027.

Yang, H., Qi, J., Xu, X., Yang, D., Lv, H., 2014. The regional variation in climate elasticity and climate contribution to runoff across China. J. Hydrol. 517, 607–616. https://doi.org/10.1016/j.jhydrol.2014.05.062.

Yang, S., 2014. Long-term changes in rainfall over eastern china and large-scale atmospheric circulation associated with recent global warming long-term changes in rainfall over eastern china and large-scale atmospheric circulation associated with recent global warming. J. Clim. 23, 1544–1562. https://doi.org/10.1175/2009JCLI2660.1.

Yao, N., Li, L., Feng, P., Feng, H., Li Liu, D., Liu, Y., Jiang, K., Hu, X., Li, Y., 2020. Projections of drought characteristics in China based on a standardized precipitation and evapotranspiration index and multiple GCMs. Sci. Total Environ. 704, 1–18. https://doi.org/10.1016/j.scitotenv.2019.135245.

Yao, N., Linchao, Li, Puyu, Feng, Hao, Feng, De Li, Liu, Yang, Liu, Xiaotao, Hu, Yi, Li, Li, L., Feng, P., Feng, H., Liu, D.Li, Liu, Y., Jiang, K., Hu, X., Li, Y., 2019. Projections of drought characteristics in China based on a standardized precipitation and evapotranspiration index and multiple GCMs College of Water Resources and Architectural Engineering, Northwest Agriculture and Forestry Key Lab of Agricultural Wate. Sci. Total Environ. https://doi.org/10.1016/j.scitotenv.2019.135245.

Yazdandoost, F., Moradian, S., Izadi, A., 2020. Evaluation of water sustainability under a changing climate in Zarrineh River Basin, Iran. Water Resour. Manag. 34, 4831–4846. https://doi.org/10.1007/s11269-020-02693-3.

Zhai, P., Zhang, X., Canada, E., Wan, H., Canada, E., Pan, X., 2005. Trends in total precipitation and frequency of daily precipitation extremes over trends in total precipitation and frequency of daily precipitation extremes over China. J. Clim. 18, 2013–2015. https://doi.org/10.1175/JCLI-3318.1.

Zhang, J., Zhang, Y., Qin, S., Wu, B., Wu, X., Zhu, Y., Shao, Y., Gao, Y., Jin, Q., Lai, Z., 2018. Effects of seasonal variability of climatic factors on vegetation coverage across drylands in northern China. L. Degrad. Dev. 29, 1782–1791. https://doi.org/10.1002/ldr.2985.

Zhang, Q., Singh, V.P., Sun, P., Chen, X., Zhang, Z., Li, J., 2011. Precipitation and streamflow changes in China: changing patterns, causes and implications. J. Hydrol. 410, 204–216. https://doi.org/10.1016/j.jhydrol.2011.09.017.

Zhang, Y., You, Q., Chen, C., Ge, J., 2016. Impacts of climate change on stream flows under RCP scenarios:a case study in Xin River Basin,China. Atmos. Res. 178–179, 521–534. https://doi.org/10.1016/j.atmosres.2016.04.018.

Zheng, H., Chiew, F.H.S., Charles, S., Podger, G., 2018. Future climate and runoff projections across South Asia from CMIP5 global climate models and hydrological modelling. J. Hydrol. Reg. Stud. 18, 92–109. https://doi.org/10.1016/j.ejrh.2018.06.004.

Zheng, J., Sun, G., Li, W., Yu, X., Zhang, C., Gong, Y., Tu, L., 2015. Impacts of land use change and climate variations on annual inflow into the Miyun Reservoir, Beijing, China. https://doi.org/10.5194/hess-20–1561-2016.

Zhu, B., Xie, X., Meng, S., Lu, C., Yao, Y., 2020. Sensitivity of soil moisture to precipitation and temperature over China: present state and future projection. Sci. Total Environ. 705, 135774 https://doi.org/10.1016/j.scitotenv.2019.135774.